Subcortical tau is linked to hypoperfusion in connected cortical regions in 4-repeat tauopathies

Sebastian N. Roemer,[1,2,†] Matthias Brendel,[3,4,5,†] Johannes Gnoerich,[4] Maura Malpetti,[6] Mirlind Zaganjori,[4] Andrea Quattrone,[7] Mattes Gross,[2,4] Anna Steward,[2] Anna Dewenter,[2] Fabian Wagner,[2] Amir Dehsarvi,[2] Christian Ferschmann,[4] Stephan Wall,[4] Carla Palleis,[1,3,5] Boris S. Rauchmann,[8,9] Sabrina Katzdobler,[1] Alexander Jaeck,[1] Anna Stockbauer,[1] Urban M. Fietzek,[1] Alexander M. Bernhardt,[1,5] Endy Weidinger,[1] Andreas Zwergal,[1,10] Sophia Stoecklein,[11] Robert Perneczky,[3,5,9,12,13] Henryk Barthel,[14] Osama Sabri,[14] Johannes Levin,[1,3,5,‡] Guenter U. Hoeglinger[1,5,‡] and Nicolai Franzmeier[2,3,15,‡]

[†,‡]**These authors contributed equally to this work.**

Abstract

4-repeat (4R) tauopathies are neurodegenerative diseases characterized by cerebral accumulation of 4R tau pathology. The most prominent 4R-tauopathies are progressive-supranuclear-palsy (PSP) and corticobasal-degeneration (CBD) characterized by subcortical tau accumulation and cortical neuronal dysfunction, as shown by PET-assessed hypoperfusion and glucose hypometabolism. Yet, there is a spatial mismatch between subcortical tau deposition patterns and cortical neuronal dysfunction, and it is unclear how these two pathological brain changes are interrelated. Here, we hypothesized that subcortical tau pathology induces remote neuronal dysfunction in functionally connected cortical regions to test a pathophysiological model that mechanistically links subcortical tau accumulation to cortical neuronal dysfunction in 4R tauopathies.

We included 51 Aβ-negative patients with clinically diagnosed PSP variants (n=26) or Corticobasal Syndrome (CBS; n=25) who underwent structural MRI and ^{18}F-PI-2620 tau-PET. ^{18}F-PI-2620 tau-PET was recorded using a dynamic one-stop-shop acquisition protocol, to determine an early 0.5-2.5 min post-tracer-injection perfusion window for assessing cortical neuronal dysfunction, as well as a 20-40 min post-tracer-injection window to determine 4R-tau load. Perfusion-PET (i.e. early-

window) was assessed in 200 cortical regions, and tau-PET was assessed in 32 subcortical regions of established functional brain atlasses. We determined tau epicenters as subcortical regions with highest ^{18}F-PI-2620 tau-PET signal and assessed the connectivity of tau epicenters to cortical ROIs using a resting-state fMRI-based functional connectivity template derived from 69 healthy elderly controls from the ADNI cohort. Using linear regression, we assessed whether i) higher subcortical tau-PET was associated with reduced cortical perfusion and ii) whether cortical perfusion reductions were observed preferentially in regions closely connected to subcortical tau epicenters.

As hypothesized, higher subcortical tau-PET was associated with overall lower cortical perfusion, which remained consistent when controlling for cortical tau-PET. Using group-average and subject-level PET data, we found that the seed-based connectivity pattern of subcortical tau epicenters aligned with cortical perfusion patterns, where cortical regions that were more closely connected to the tau epicenter showed lower perfusion.

Together, subcortical tau-accumulation is associated with remote perfusion reductions indicative of neuronal dysfunction in functionally connected cortical regions in 4R-tauopathies. This suggests that subcortical tau pathology may induce cortical dysfunction, which may contribute to clinical disease manifestation and clinical heterogeneity.

Author affiliations:

1 Department of Neurology, University Hospital, LMU Munich, 81377 Munich, Germany

2 Institute for Stroke and Dementia Research (ISD), University Hospital, LMU Munich, 81377 Munich, Germany

3 Munich Cluster for Systems Neurology (SyNergy), 81377 Munich, Germany

4 Department of Nuclear Medicine, University Hospital, LMU Munich, 81377 Munich, Germany

5 German Center for Neurodegenerative Diseases (DZNE) Munich, Munich, 81377 Munich, Germany

6 Department of Clinical Neurosciences, University of Cambridge, CB2 1TN Cambridge, UK

7 Institute of Neurology, Magna Graecia University, 88100 Catanzaro, Italy.

8 Department of Neuroradiology, University Hospital, LMU Munich, 81377 Munich, Germany

9 Department of Psychiatry and Psychotherapy, University Hospital, LMU Munich, 80336 Munich, Germany

10 German Center for Vertigo and Balance Disorders (DSGZ), University Hospital, LMU Munich, 81377 Munich, Germany

11 Department of Radiology, University Hospital, LMU Munich, 81377 Munich, Germany

12 Aging Epidemiology (AGE) Research Unit, School of Public Health, Imperial College London, SW7 2BX London, UK

13 Sheffield Institute for Translational Neuroscience (SITraN), University of Sheffield, S10 2HQ Sheffield, UK

14 Department of Nuclear Medicine, University Hospital of Leipzig, 04103 Leipzig, Germany

15 University of Gothenburg, The Sahlgrenska Academy, Institute of Neuroscience and Physiology, Department of Psychiatry and Neurochemistry, SE 413 90 Mölndal and Gothenburg, Sweden

Correspondence to: Dr Nicolai Franzmeier

Feodor-Lynen Str. 17

81371 Munich, Germany

E-mail: nicolai.franzmeier@med.uni-muenchen.de

Running title: Tau versus perfusion-PET in 4R tauopathies

Keywords: PI-2620 tau-PET; 4R-tauopathies; PSP; CBD; functional connectivity; perfusion-PET

Introduction

Four-Repeat (4R) tauopathies are rapidly progressive neurodegenerative diseases characterized by neuronal and glial aggregation of hyperphosphorylated 4R tau, that most commonly manifest as

progressive supranuclear palsy (PSP) and cortico-basal syndrome (CBS) with mixed subcortical and cortical symptoms [1-4].

Neuropathological studies have shown that 4R tau accumulates initially in subcortical and brainstem structures, congruent with the early-stage clinical manifestation of subcortical symptoms as well as MRI-assessed atrophy across subcortical and brainstem structures [5]. In contrast, 4R tau aggregation in cortical regions is less pronounced and typically found later in more advanced disease stages [6-10]. We recently aimed to recapitulate *in vivo* spreading patterns of 4R tau in clinically diagnosed PSP and CBS patients (i.e. amyloid-negative to rule out confounding Alzheimer's type 3/4R tau pathology), using ^{18}F-PI-2620 tau-PET which shows binding affinity to 4R tau deposits in autoradiography studies, molecular simulations and *in vitro* competition assays [11-16]. In line with post mortem studies, we found elevated ^{18}F-PI-2620 tau-PET binding to be most pronounced in subcortical structures (i.e. basal ganglia) while cortical ^{18}F-PI-2620 tau-PET increase was more limited in these patients [16-19]. These converging neuropathological and neuroimaging findings support the view that 4R tau aggregation targets primarily subcortical structures [9,18]. In contrast, FDG-PET or perfusion-PET studies assessing neuronal dysfunction in 4R tauopathy patients found that hypoperfusion or glucose hypometabolism extend majorly beyond the typical subcortical 4R tau predilection sites into the cortex [17,20-24]. This suggests that 4R tauopathy patients develop neuronal dysfunction beyond the sites of primary tau pathology, which may give rise to additional cortical symptoms characteristic for PSP and CBS [17]. However, it is unclear whether and how subcortical tau pathology and cortical neuronal dysfunction are inter-related, i.e. whether subcortical tau pathology actively promotes neuronal dysfunction in the cortex [23,24]. To address this, we adapted the concept of remote dysfunction that is well-known in stroke research, which explains reduced function of a given brain region by the lack of input of a spatially remote yet connected area [25-28]. Specifically, we hypothesized that subcortical tau deposition in 4R tauopathy patients acts as a spatially circumscribed lesion that induces remote neuronal dysfunction in connected cortical areas, thereby mechanistically linking subcortical tau deposition and cortical neuronal dysfunction. We addressed this in a sample of 51 Aβ-negative patients with clinically diagnosed PSP variants (PSP Richardson Syndrome: n=19; PSP Progressive Gait Freezing: n=1; PSP Parkinsonism: n=2; PSP Speech/Language Variant: n=4) or CBS (n=25) (i.e. amyloid-negative), all of whom underwent full dynamic 60-minute ^{18}F-PI-2620 tau-PET scanning and structural MRI at the LMU University Hospital in Munich, Germany. Using the 60-minute

dynamic ^{18}F-PI-2620 tau-PET scanning protocol, we used a one-stop-shop protocol previously established by us to i) determine late-phase tracer binding as a marker of 4R tau deposition, and ii) to assess perfusion-phase images right after tracer injection as a proxy of neuronal dysfunction that is closely correlated with ^{18}F-FDG-PET [17,29,30]. This cutting-edge dynamic imaging protocol enabled a simultaneous assessment of both tau deposition and perfusion during a single PET-scanning session, facilitating the assembly of a large 4R-tauopathy cohort and yielding two complementary image modalities. To model brain connectivity between subcortical sites of tau deposition and cortical sites of neuronal dysfunction, we used a previously established functional connectivity template determined in 69 healthy controls of the ADNI sample with high-resolution resting-state fMRI [16,31,32]. Using these data, our key aims were to test i) whether PET-assessed subcortical tau deposition is generally linked to cortical hypoperfusion, ii) whether cortical hypoperfusion is observed specifically in those brain regions that are functionally connected to subcortical epicenters of 4R tau pathology and iii) whether patient-specific subcortical tau epicentre connectivity patterns align with corresponding cortical hypoperfusion patterns.

Materials and methods

Sample

We included a total of 51 subjects with clinically diagnosed PSP variants (n=26: PSP Richardson Syndrome: n=19; PSP Progressive Gait Freezing: n=1; PSP Parkinsonism: n=2; PSP Speech/Language Variant: n=4) or CBS (n=25) who underwent structural 3T T1-weighted MRI and fully dynamic ^{18}F-PI-2620 tau-PET with 4R tau as the assumed underlying pathology of the clinical phenotypes. PSP was diagnosed following state-of-the-art diagnostic criteria [2]. CBS diagnosis was made according to the revised Armstrong Criteria of probable CBS [33] or the Movement Disorders Society criteria of possible PSP with predominant CBS [2]. Inclusion criteria were age above 45 years, stable pharmacotherapy for at least 1 week before PET scanning, no family history for Parkinson's or Alzheimer's disease. Exclusion criteria were severe neurological or psychiatric disorders with phenotypes other than other than PSP and CBS or positive Aβ status, (i.e. to exclude Alzheimer's disease-type tau pathology) as determined via expert visual read of ^{18}F-Flutemetamol or ^{18}F-florbetaben amyloid-PET or by cerebrospinal fluid analyses of Aβ

biomarker levels using locally established cut-offs (i.e., Aβ42/40-ratio<5.5 or $A\beta_{1-42}$<375pg/ml). Written informed consent was obtained from all participants. The study was carried out according to the principles of the Helsinki Declaration, patients received no compensation for study participation. The full study protocol was approved by the local ethics committee (LMU Munich, application numbers 17-569 and 19-022) and the German radiation protection authorities (BfS-application: Z 5 − 22464/2017-047-K-G).

Neuroimaging acquisition and image preprocessing

All patients underwent T1-weighted structural MRI on a 3T Siemens Magnetom PRISMA or SKYRA Scanner and ^{18}F-PI-2620 tau-PET in a full dynamic setting (0–60 min post-injection) using pre-established standard PET scanning parameters [15]. A detailed description of our in-house ^{18}F-PI-2620 synthesis and quality control pipeline has been described previously [16,18]. Dynamic ^{18}F-PI-2620 tau-PET imaging was acquired on a Siemens Biograph True point 64 PET/CT (Siemens, Erlangen, Germany) or a Siemens mCT scanner (Siemens, Erlangen, Germany) in 3D list-mode over 60 min together with a low dose CT for attenuation correction. From the dynamic PET image acquisition, we reconstructed early-phase perfusion-PET images during 0.5–2.5 min p.i. and late-phase tau-PET images for 20-40min p.i. and summarized perfusion and late-phase tau-PET into a single frame after motion correction, respectively [15,17,29,30].

All imaging data were processed using the Advanced Normalization Tools (ANTs) toolbox (http://stnava.github.io/ANTs/). In an initial step, ^{18}F-PI-2620 perfusion-PET and tau-PET images were rigidly co-registered to native-space T1-weighted MRI images. For T1-weighted structural MRI data we performed bias field correction, brain extraction, and segmentation into gray-matter, white matter and cerebrospinal fluid tissue maps using the ANTs cortical thickness pipeline. Brain extracted T1-weighted images were nonlinearly normalized to MNI space using ANTs high-dimensional warping algorithm [34]. By combining the rigid PET to T1-native space and nonlinear T1 to MNI space spatial normalization parameters, all brain-atlas-derived ROI data was transformed from MNI space back to PET native space, including the TIAN 32 ROI subcortical brain atlas, the Schaefer 200 ROI cortical brain atlas, as well as reference regions (i.e. inferior cerebellum for tau-PET and pons for perfusion-PET) in line with our previous studies [16,35,36]. We specifically selected the TIAN and Schaefer atlases since they were established using fMRI to

optimally capture homogeneous functional brain units rendering them ideal for combining PET and fMRI data and to maximize consistency with our previous studies in which we used these atlases.[16,31,32,37-43] A mean overlay of the inferior cerebellar reference ROI on the group-average tau-PET image (i.e. 20-40minute SUVR) in MNI space is shown in Supplementary Fig.1, to illustrate that the reference ROI does not overlap with sites of off-target binding in the dentate nucleus of the cerebellum. All brain-atlas data and the inferior cerebellar reference ROI were further masked with binary subject-specific gray-matter maps to restrict later extraction of ROI-mean values to gray-matter regions and to avoid signal spill in from adjacent white matter or CSF regions. Mean ROI values were extracted for the TIAN and Schaefer ROIs and z-score normalized to an in-house reference sample of 9 healthy control subjects (mean±SD age=72.2±10.51, female/male=4/5). Mean distributions of the resulting cortical and subcortical perfusion and tau-PET z-scores in the patient cohort are shown in Supplementary Fig.2, illustrating the presence of both abnormal perfusion-PET (i.e. z-zscore below -1.5) and abnormal tau-PET (i.e. z-score above 1.5). All statistical analyses described in the manuscript were performed on z-score transformed PET SUVRs. To determine the robustness of our findings, we also determined DVR-based z-scores scores using kinetic modelling (i.e. STRM2) as implemented in the Qmodeling software package.[44]

For assessing functional connectivity between the 200 Schaefer and 32 TIAN ROIs, we used 3T resting-state fMRI data from 69 cognitively normal controls of the ADNI cohort that had no evidence of clinically relevant cerebral amyloid or tau pathology, as indicated by negative ^{18}F-florbetapir amyloid-PET (i.e. global SUVR<1.11) [45] and negative ^{18}F-flortaucipir tau-PET scans (i.e. global SUVR<1.3) [46]. An in-depth description of the resting-state fMRI acquisition parameters, preprocessing and methods to determine functional connectivity has been published previously by us [16]. Consistent with our previous studies, the functional connectivity matrix was thresholded at 30% to eliminate negative and noisy connections, and transformed to connectivity-based distance where shorter distance indicates stronger connectivity.[31,37,38]

Statistics

To assess whether subcortically elevated ^{18}F-PI-2620 tau-PET binding signal is associated with reduced cortical perfusion-PET, we used linear regression, controlling for age and sex. Additional

models were run controlling for ^{18}F-PI-2620 tau-PET binding signal averaged across all cortical ROIs, to ensure that associations between subcortical tau and cortical hypoperfusion are not driven by concomitant cortical tau deposition. Furthermore, ROI-wise linear regressions were carried out to assess if regional perfusion-PET reductions are associated with higher subcortical ^{18}F-PI-2620 tau-PET binding signal, controlled for age, sex and ^{18}F-PI-2620 tau-PET binding signal in the corresponding cortical ROI. To adjust for multiple comparisons across the 200 cortical ROIs, p-values were FDR-corrected at an alpha level of 0.05. To determine whether cortical hypoperfusion patterns followed the connectivity of subcortical tau epicenters on the group-level, we assessed 10% of subcortical regions with the highest tau-PET z-scores and assessed their mean functional connectivity-based distance to the 200 cortical ROIs using according to the ADNI-derived functional connectivity template. Using linear regression, we then tested whether tau epicenter connectivity was associated with cortical perfusion-PET z-scores, controlling for tau-PET z-scores in corresponding cortical ROIs. The same analyses were also performed at the subject level, by defining 10% of subcortical regions with the highest tau-PET signal as patient-specific epicenters and usage of cortical perfusion-PET z-scores on subject level. Beta-values of the subject-level regression-derived association between tau epicenter connectivity and cortical perfusion-PET were extracted across the 51 subjects. To determine whether beta-values were significantly different from zero, we performed a one-sample t-test and obtained 95% confidence intervals across the regression-derived beta values.

Lastly, we tested whether regions with strongest hypoperfusion can be predicted on the subject-level. To this end, we adopted a pre-established approach that organizes cortical regions into four quartiles, depending on their connectivity to the subject-level tau epicenter (i.e. Q1=strongest connectivity to the tau epicenter vs. Q4=weakest connectivity to the tau epicenter) [31,47,48]. We determined mean perfusion-PET z-scores in Q1-Q4 ROIs for each subject and determined differences between Q1-Q4 perfusion-PET z-scores using paired t-tests. Statistical analyses were computed using R statistical software version 4.0.2 http://www.R-project.org; [49]

Results

The final sample included 51 patients with clinical diagnosis of PSP variants (n=26) or CBS (n=25) and negative amyloid-biomarker status to rule out confounding AD-type 3/4R tau pathology.

Group-mean renderings of abnormality in cortical perfusion-PET (i.e. adjusted to a pons reference region) and tau-PET (i.e. adjusted to an inferior cerebellar reference region) are shown in Fig. 1A&B, illustrating abnormal tau-PET signal (i.e. z-scores falling above 1.5) in subcortical and primary sensorimotor regions, as well as hypoperfusion (i.e. z-scores falling below -1.5) in cingulate and lateral frontal brain regions, in line with previous studies [16-18,20-24]. Group-average slice-view tau-PET images are shown in supplementary Figure 3. Sample demographics and clinical characteristics can be found in **Table 1**.

Higher subcortical tau-PET is associated with global cortical perfusion reductions

To address our first aim, we investigated whether higher tau-PET signal in subcortical epicenters of tau pathology are associated with an overall reduction in cortical perfusion-PET. To this end, we identified patient-specific tau epicenters (i.e. 10% of subcortical brain regions with highest tau-PET z-scores) and averaged the tau-PET SUVR z-scores across subcortical tau epicenters. To determine overall cortical perfusion, we averaged the perfusion-PET SUVR z-scores across the 200 cortical Schaefer ROIs. Using linear regression, we could confirm that higher ^{18}F-PI-2620 tau-PET binding signal in subcortical epicenters is indeed linked to lower cortical perfusion-PET, controlling for age and sex (β=-0.263, p=0.038, Fig.2A). This association was consistent when additionally controlling for average cortical tau-PET SUVR z-scores (i.e. the mean across the 200 Schaefer ROIs; β=-0.361; p=0.009), or when additionally altering the etau picenter threshold (5/15/20%: b=-0.333/-0.375/-0.387, p=0.016/0.007/0.006), indicating that associations between subcortical tau and cortical hypoperfusion are not specifically driven by concomitant cortical ^{18}F-PI-2620 tau-PET increases or by the specific size definition of the epicenter. These results remained consistent when determining tau epicenters based on DVR-based z-scores instead of SUVRs (Supplementary Fig.4A). We also determined linear models to test the association between subcortical tau and cortical perfusion for each of the 200 cortical ROIs, controlling for age, sex and cortical tau of the corresponding ROI. Here, we found that higher subcortical ^{18}F-PI-2620 tau-PET signal was associated with lower perfusion in widespread bilateral association cortices after FDR-correction for multiple comparisons, with strongest effects found in medial and lateral frontal regions (Fig.2B, replication using DVR-based tau-PET z-scores shown in Supplementary Fig.4B). Importantly, these results were independent of local cortical tau-PET levels. Overall, these results

support the hypothesis that subcortical tau-PET increase, i.e. indicative of higher 4R tau pathology, is associated with reduced perfusion as a marker of neuronal dysfunction in the cortex.

Cortical perfusion patterns follow the connectivity of subcortical tau epicenters

To address our second aim, we determined whether elevated tau-PET in the subcortex is specifically linked to reduced perfusion-PET in those cortical regions that are most connected to the subcortical tau epicenter. To this end, we defined group-average tau-PET and perfusion-PET patterns and determined 10% of subcortical ROIs with highest tau-PET z-scores signal the epicenters of tau pathology (Fig.3A). Next, we used the functional connectivity template derived from 69 healthy elderly controls and determined the connectivity-based distance of the group-level tau epicenters to the 200 cortical Schaefer ROIs (Fig.3B). Using linear regression, we found that connectivity of the subcortical tau epicenters indeed aligned with cortical perfusion-PET patterns (Fig.3C), where regions that were more closely connected to the tau epicenters showed overall lower perfusion (β=0.637, p<0.001, R^2=0.41; Fig.3D). Again, this result pattern remained consistent when controlling for cortical tau-PET in corresponding ROIs (β=0.565, p<0.001, R^2=0.32; Fig.3D), suggesting that lower cortical perfusion is linked to tau in connected subcortical tau epicenters rather than cortical tau. Again, these results were consistent when changing the size definition of the epicenter (i.e. 5/15/20%, b=0.533/0.544/0.445, p<0.001 for all thresholds), or when using DVR-based tau-PET z-scores to define tau epicenters (Supplementary Fig.5A).

Patient-level cortical hypoperfusion follows the connectivity of subcortical tau epicenters

To address our third aim, we determined whether the link between tau epicenter connectivity and lower cortical perfusion can be recapitulated on the subject-level, and therefore explain inter-individual heterogeneity in tau deposition and cortical perfusion patterns. Therefore, we applied the above-described approach to patient level tau-PET and perfusion-PET data. Specifically, we determined tau-epicenters (i.e. 10% of subcortical ROIs with highest tau-PET) for each patient and extracted seed-based functional connectivity-based distance of these tau epicenters to the 200 cortical ROIs using the connectivity template. We then used subject-specific linear regression models to assess whether the connectivity-based distance of the tau epicenters was associated with

cortical perfusion while controlling for tau-PET in corresponding cortical ROIs and extracted subject-level standardized regression coefficients (i.e. β-values). The mean standardized β-coefficients of the association between epicenter connectivity and cortical perfusion were significantly greater than zero (mean: 0.142; 95% CI [0.072;0.212], t(50)=4.06, p<0.001, Fig.3E), supporting the hypothesis that reduced cortical perfusion is observed predominantly in regions that are functionally most closely connected to the tau epicenters in 4R tauopathies. This result was further confirmed using linear mixed models across subjects, using epicenter connectivity as a predictor of cortical perfusion, controlling for age, sex and random intercept (b/SE=0.172/0.01, T=16.303, p<0.001). To illustrate this concept further, we assessed subject level cortical perfusion-PET grouped into four quartiles depending on the connectivity to the tau epicenter (i.e. Q1=strongest connectivity to the subcortical tau epicenter vs. Q4=weakest connectivity to the tau epicenter, Fig.4). In line with the previous analyses, we found that cortical perfusion-PET reductions followed the connectivity of the subcortical tau epicenters, with strongest perfusion reduction in Q1 whereas the perfusion deficit became weaker across Q2-Q4 regions (Fig.4). All results remained consistent when altering the tau epicenter threshold between 5-20% or when using DVR-based tau-PET z-scores to determine tau epicenters (Supplementary Fig.5B&C). Overall, these findings provide converging evidence that subject-level patterns of cortical hypoperfusion in 4R tauopathy patients follow the connectivity pattern of subcortical tau epicenters, with strongest perfusion reductions in those brain regions that are most closely connected to a given individuals tau epicenter.

Discussion

Using a fully dynamic ^{18}F-PI-2620 tau-PET scanning protocol to simultaneously model cerebral perfusion and tau deposition, we confirmed previous evidence that PSP and CBS patients with clinically suspected 4R tauopathies show predominant subcortical tau-PET increase [16,18,50], while perfusion reductions extend into the cortex beyond the primary sites of PET-assessed 4R tau deposition [9,17,21,22,29]. Based on these initial confirmatory results, our key aim was to determine whether subcortical 4R tau deposition induces cortical hypoperfusion in spatially remote but connected brain regions. Supporting this, our main findings were first, that elevated subcortical ^{18}F-PI-2620 tau-PET was indeed associated with overall reduced cortical perfusion-PET levels and

second, that the patterns of cortical hypoperfusion specifically followed the resting-state fMRI-assessed functional connectivity patterns of those subcortical epicenter regions. Thirdly, we found that patient-specific reductions in cortical perfusion were most prominent in those regions that had the strongest connectivity to a given subjects' subcortical tau epicenter. In summary, these findings provide *in vivo* evidence for a mechanistic model of 4R tauopathy-related brain changes, showing that subcortical tau deposition may induce remote neuronal dysfunction in connected cortical regions which may explain the complex clinical manifestation of cortical and subcortical symptoms in PSP and CBS [17].

For our first major finding, we report that elevated subcortical tau deposition is linked to overall lower cortical perfusion levels, particularly in lateral frontal and cingulate predilection sites of hypoperfusion or glucose hypometabolism that have been previously described in 4R tauopathy patients [17,20,21]. Importantly, these results remained fully consistent when statistically controlling for tau-PET levels in corresponding cortical regions, indicating that more abnormal subcortical tau-PET levels explain cortical hypoperfusion beyond putative co-occurring cortical tau pathology [17,20,21,29,51,52]. Subcortical predilection sites for 4R tau deposition such as the basal ganglia have widespread connections to the cortex, embedded in complex neuronal circuits involved in movement, arousal, and cognitive functions [53,54]. Subcortical damage induced by neurotoxic 4R tau deposits may therefore induce disbalance within cortico-subcortical circuits that manifest as dysfunction in cortical regions that are not yet directly affected by severe tau deposition [9,55,56]. This view is conceptually in line with previous neuroimaging studies showing remote cortical glucose hypometabolism, hypoperfusion and cortical symptoms following subcortical stroke, together supporting the view that subcortical damage can manifest in spatially remote cortical dysfunction and associated clinical deficits [57-59].

Beyond a mere association between subcortical tau deposition and cortical hypoperfusion, our results illustrate further, that cortical hypoperfusion patterns specifically follow the functional connectivity of those subcortical brain regions with strongest tau deposition (i.e. epicenters). Here, group-level mappings indicate that the subcortical tau epicenters show strongest connectivity to anterior cingulate and lateral frontal brain regions, i.e. regions that had on average also the strongest reduction in perfusion-PET in line with previous studies (i.e. see Figure 3) [20,21]. In

contrast, more posterior brain regions with weak connectivity to the tau epicenters showed relatively preserved cortical perfusion. Supporting the robustness and generalizability of this mechanistic association, the associations between tau epicenter connectivity and hypoperfusion patterns were replicable for subject-level PET data, suggesting that the heterogeneity in subcortical tau deposition and cortical hypoperfusion patterns are potentially explained by variable connectivity patterns of subcortical epicenters of 4R tau aggregation [60]. This is further supported by our finding that subject-specific cortical sites of strongest perfusion reductions could be predicted by identifying those brain regions that were most closely connected to a given subjects tau epicenter (i.e. Q1). Therefore, a connectomic framework to cross-link tau deposition and neuronal dysfunction on the patient level may be a promising future approach to guide personalized neuroimaging readouts to improve the detection of therapeutic effects on neuronal dysfunction in clinical trials, as previously suggested by us and others for Alzheimer's disease [38,61]. From a mechanistic point of view, our results provide critical support for the hypothesized remote development of cortical dysfunction in 4R tauopathy patients, where 4R tau associated subcortical damage induces dysfunction particularly in spatially remote but nevertheless closely connected brain regions. Since we reported previously that cortical hypoperfusion rather than subcortical ^{18}F-PI-2620 tau-PET increases are associated with symptom severity in PSP [17,18], it will be a key next step to assess whether cortical dysfunction associated with subcortical tau deposition can explain the extensive heterogeneity in clinical symptom manifestation across 4R tauopathies [2,62].

A key strength of the current study is that all associations between cortical hypoperfusion and connectivity of subcortical tau epicenters were statistically controlled for cortical tau deposition, thereby fortifying the concept of remote cortical hypoperfusion rather than simply being explained by co-localized cortical tau deposition. Controlling for cortical tau levels is a critical step, since we previously showed that brain-wide tau deposition patterns assessed *in vivo* via ^{18}F-PI-2620 tau-PET or post-mortem also follow the seed-based connectivity of tau epicenters, in line with previous evidence that tau spreads across synaptic connections similar to AD [16,38,63-65]. Yet, our current results suggest that cortical hypoperfusion is not fully explained by the spreading of tau from the subcortex to connected cortical regions, but further aggravated by altered communication with subcortical tau epicenters. Therefore, it will be an important next step to characterize how subcortical tau deposition alters neuronal signalling and communication with cortical regions, thereby introducing changes in cortical perfusion. Addressing this question may help identify

therapeutic approaches to reduce the impact of subcortical tau on cortical dysfunction, which may translate into attenuated clinical disease manifestation and progression [17]. Furthermore, the deeper mechanistic understanding of cortical dysfunction due to altered neuronal communication to subcortical regions affected by tau may help establish novel read-outs in clinical trials. With cortical neuronal dysfunction potentially constituting the bridge between subcortical tau accumulation and clinical symptomatology [17], individual cortical hypoperfusion patterns could be used to objectively assess effects of tau reducing treatments and their impact on clinical presentation. An additional strength is the usage of a pre-established cutting-edge ^{18}F-PI-2620 PET neuroimaging protocol that allows simultaneous assessment of tau deposition and cerebral perfusion as a marker of neuronal dysfunction in the same scanning session, thereby minimizing bias introduced by day-to-day physiological and technical variability [17,29,60]. In addition, we have performed extensive *in vivo* neuroimaging, post mortem autoradiographic and in vitro competition assay analyses that support the capability of ^{18}F-PI-2620 to bind to 4R tau fibrils, particularly in relatively early imaging windows 20-40 minutes after tracer injection, rendering ^{18}F-PI-2620 a promising tracer for *in vivo* imaging of 4R tau [13,15,16,18,66]. Further, we have shown that early-phase ^{18}F-PI-2620 perfusion imaging yields comparable results to perfusion imaging with amyloid-PET tracers and ^{18}FDG-PET, overall supporting the feasibility of early-phase perfusion-PET protocols to assess neuronal dysfunction in 4R tauopathy patients [29,60].

However, several limitations should also be highlighted for the interpretation of the current results. To date, a final diagnosis of 4R tauopathies can only be made post-mortem, hence inclusion for the current study was exclusively based on established clinical criteria for the diagnosis of PSP and CBS [2,33]. By excluding amyloid-biomarker (i.e. PET or CSF) positive patients, we aimed to limit the likelihood of concomitant AD-type 3/4R tau pathology, and to maximize the likelihood of 4R tau as an underlying cause of clinical symptoms, however, we cannot fully exclude the confound of other pathologies other than 4R tau on our current results until biomarker-based diagnosis of 4R tauopathies is fully established. Further, it is not entirely clear how sensitive PI-2620 binds to intracellular tau deposits in vital cells, or whether only tau deposits left behind by dead cells are visualized. Addressing this in future studies will be important to further determine at what stage 4R deposits can be visualized with PI-2620. In addition, we did not assess associations between clinical heterogeneity, cortical perfusion, and subcortical tau deposition, due to limited availability of clinical scores in the current sample (see table 1). Also, overall perfusion

reductions are relatively low in the current sample, so that a clinically more advanced patient collective would be desirable to replicate the current findings. However, we caution that clinically more advanced patients may be more difficult to recruit for a relatively demanding MRI and PET-imaging protocol. Further, we employed resting-state fMRI as a marker of connectivity, which is determined based on shared inter-regional BOLD activity, and overlaps to a large degree, but not fully, with structural connectivity assessed via diffusion MRI [67]. We specifically used functional connectivity due to its well-established ability to assess subcortical to cortical connectivity and to map multi-synaptic connections which may underlie the remote neuronal dysfunction that are typically not captured by diffusion imaging [25,68,69]. Additionally, as in several of our previous studies, resting-state fMRI templates were derived from healthy controls of another dataset, since resting-state fMRI data were not systematically collected in the current sample [16,31,32,47,65]. This connectivity template does not capture inter-individual variability in functional connectivity, as well as possible disease-related connectivity changes, which both might exert an influence on cortical neuronal dysfunction patterns induced by subcortical tau deposition. Thus, we are currently collecting high quality subject level resting-state fMRI data (i.e. connectome fingerprinting), to determine in a next step whether subject-level functional connectivity patterns change in 4R-tauopathy patients, and explain the heterogeneity of cortical dysfunction to a greater extent [70]. Lastly, the current study followed a cross-sectional study design and is consequently unable to reveal the suggested temporal sequence of subcortical tau accumulation and cortical dysfunction. To support the concept of a remote cortical dysfunction as a consequence of subcortical tau-accumulation, future longitudinal studies are needed, which are currently initiated at our site.

Together, our results strongly suggest that subcortical tau deposition can induce cortical neuronal dysfunction in connected regions in 4R tauopathies. To our knowledge this is the first patient study to establish a mechanistic relationship between two hallmark neuroimaging markers of 4R tauopathies, i.e. cortical dysfunction and subcortical tau deposition, which is critical for understanding pathophysiological mechanisms and inter-individual variability in disease manifestation. The remote cortical dysfunction in 4R tauopathy patients described in this study could therefore serve as an imaging-guided readout to estimate treatment-effects in clinical trials targeting tau pathology or its downstream effects on neuronal integrity and function.

Data availability

The data are available upon request from the corresponding author to qualified academic investigators for the sole purpose of replicating procedures and results presented in the article and as long as data transfer is in agreement with EU legislation on the general data protection regulation and decisions by the Ethical Review Board of the LMU University hospital.

Funding

N.F. was funded by the German Parkinson Society (DPG). J.L., G.H., N.F. and M.B. were funded by the Deutsche Forschungsgemeinschaft (DFG) under Germany's Excellence Strategy within the framework of the Munich Cluster for Systems Neurology (EXC 2145 SyNergy – ID 390857198). G.H. was funded by the German Federal Ministry of Education and Research (BMBF, 01EK1605A HitTau). J.L., S.K. and C.P. received research funding from Lüneburg heritage.

Competing interests

Johannes Levin reports speaker fees from Bayer Vital, Biogen, EISAI, TEVA, Zambon and Roche, consulting fees from Axon Neuroscience, EISAI and Biogen, author fees from Thieme medical publishers and W. Kohlhammer GmbH medical publishers and is inventor in a patent "Oral Phenylbutyrate for Treatment of Human 4-Repeat Tauopathies" (EP 23 156 122.6) filed by LMU Munich. In addition, he reports compensation for serving as chief medical officer for MODAG GmbH, is beneficiary of the phantom share program of MODAG GmbH and is inventor in a patent "Pharmaceutical Composition and Methods of Use" (EP 22 159 408.8) filed by MODAG GmbH, all activities outside the submitted work.

Maura Malpetti "Race Against Dementia Alzheimer's Research UK (ARUK-RADF2021A-010) and the National Institute for Health Research (NIHR) Cambridge Biomedical Research Centre (NIHR203312: the views expressed are those of the authors and not necessarily those of the NIHR or the Department of Health and Social Care)."

Andreas Zwergal received speaker honoraria and research support from Dr. Willmar Schwabe GmbH.

C. Palleis is inventor in a patent "Oral Phenylbutyrate for Treatment of Human 4-Repeat Tauopathies" (EP 23 156 122.6) filed by LMU Munich and was was supported by the Deutsche Forschungsgemeinschaft (DFG, German Research Foundation) under Germany's Excellence Strategy within the framework of the Munich Cluster for Systems Neurology (EXC 2145 SyNergy – ID 390857198). The Lüneburg Heritage and Friedrich-Baur-Stiftung have supported the work of C.Palleis.

Günter Höglinger received research support from UCB and the Rainwater Charitable Foundation; has ongoing research collaborations with Roche; serves as a consultant for Abbvie, Alzprotect, Amylyx, Aprineua, Asceneuron, Bayer, Bial, Biogen, Biohaven, Epidarex, Ferrer, Kyowa Kirin, Lundbeck, Novartis, Retrotope, Roche, Sanofi, Servier, Takeda, Teva, UCB; received honoraria for scientific presentations from Abbvie, Bayer, Bial, Biogen, Bristol Myers Squibb, Kyowa Kirin, Pfizer, Roche, Teva, UCB, Zambon. holds a patent on Treatment of Synucleinopathies. United States Patent No.: US 10,918,628 B2; EP 17 787 904.6-1109 / 3 525 788; received publication royalties from Academic Press, Kohlhammer, and Thieme;

Nicolai Franzmeier received speaker honoraria from LMI and ESAI, consulting honoraria from MSD and receives research support from Eli Lilly, the Bright Focus Foundation, the Alzheimer's Association, the Alzheimer Forschung Initiative and the Hertie Foundation. All activities are outside the submitted work. The present work was supported by a Grant from the German Parkinson Foundation (DPG)

The authors report no competing interest.

Supplementary material

Supplementary material is available at *Brain* online.

References

1. Kovacs GG. Invited review: Neuropathology of tauopathies: principles and practice. *Neuropathol Appl Neurobiol*. Feb 2015;41(1):3-23. doi:10.1111/nan.12208

2. Hoglinger GU, Respondek G, Stamelou M, *et al*. Clinical diagnosis of progressive supranuclear palsy: The movement disorder society criteria. *Mov Disord*. Jun 2017;32(6):853-864. doi:10.1002/mds.26987

3. Rosler TW, Tayaranian Marvian A, Brendel M, *et al*. Four-repeat tauopathies. *Prog Neurobiol*. Sep 2019;180:101644. doi:10.1016/j.pneurobio.2019.101644

4. Constantinides VC, Paraskevas GP, Paraskevas PG, Stefanis L, Kapaki E. Corticobasal degeneration and corticobasal syndrome: A review. *Clin Park Relat Disord*. 2019;1:66-71. doi:10.1016/j.prdoa.2019.08.005

5. Carlos AF, Tosakulwong N, Weigand SD, *et al*. Histologic lesion type correlates of magnetic resonance imaging biomarkers in four-repeat tauopathies. *Brain Commun*. 2022;4(3):fcac108. doi:10.1093/braincomms/fcac108

6. Dutt S, Binney RJ, Heuer HW, *et al*. Progression of brain atrophy in PSP and CBS over 6 months and 1 year. *Neurology*. Nov 8 2016;87(19):2016-2025. doi:10.1212/WNL.0000000000003305

7. Cordato NJ, Duggins AJ, Halliday GM, Morris JG, Pantelis C. Clinical deficits correlate with regional cerebral atrophy in progressive supranuclear palsy. *Brain*. Jun 2005;128(Pt 6):1259-66. doi:10.1093/brain/awh508

8. Hoglinger GU, Schope J, Stamelou M, *et al*. Longitudinal magnetic resonance imaging in progressive supranuclear palsy: A new combined score for clinical trials. *Mov Disord*. Jun 2017;32(6):842-852. doi:10.1002/mds.26973

9. Kovacs GG, Lukic MJ, Irwin DJ, *et al*. Distribution patterns of tau pathology in progressive supranuclear palsy. *Acta Neuropathol*. Aug 2020;140(2):99-119. doi:10.1007/s00401-020-02158-2

10. Zhang Y, Wu KM, Yang L, Dong Q, Yu JT. Tauopathies: new perspectives and challenges. *Mol Neurodegener*. Apr 7 2022;17(1):28. doi:10.1186/s13024-022-00533-z

11. Malarte ML, Gillberg PG, Kumar A, Bogdanovic N, Lemoine L, Nordberg A. Discriminative binding of tau PET tracers PI2620, MK6240 and RO948 in Alzheimer's disease, corticobasal

degeneration and progressive supranuclear palsy brains. *Mol Psychiatry*. Mar 2023;28(3):1272-1283. doi:10.1038/s41380-022-01875-2

12. Kroth H, Oden F, Molette J*, et al*. Discovery and preclinical characterization of [(18)F]PI-2620, a next-generation tau PET tracer for the assessment of tau pathology in Alzheimer's disease and other tauopathies. *Eur J Nucl Med Mol Imaging*. Sep 2019;46(10):2178-2189. doi:10.1007/s00259-019-04397-2

13. Kunze G, Kumpfel R, Rullmann M*, et al*. Molecular Simulations Reveal Distinct Energetic and Kinetic Binding Properties of [(18)F]PI-2620 on Tau Filaments from 3R/4R and 4R Tauopathies. *ACS Chem Neurosci*. Jul 20 2022;13(14):2222-2234. doi:10.1021/acschemneuro.2c00291

14. Messerschmidt K, Barthel H, Brendel M*, et al*. (18)F-PI-2620 Tau PET Improves the Imaging Diagnosis of Progressive Supranuclear Palsy. *J Nucl Med*. Apr 14 2022;doi:10.2967/jnumed.121.262854

15. Song M, Scheifele M, Barthel H*, et al*. Feasibility of short imaging protocols for [(18)F]PI-2620 tau-PET in progressive supranuclear palsy. *Eur J Nucl Med Mol Imaging*. Nov 2021;48(12):3872-3885. doi:10.1007/s00259-021-05391-3

16. Franzmeier N, Brendel M, Beyer L*, et al*. Tau deposition patterns are associated with functional connectivity in primary tauopathies. *Nat Commun*. Mar 15 2022;13(1):1362. doi:10.1038/s41467-022-28896-3

17. Katzdobler S, Nitschmann A, Barthel H*, et al*. Additive value of [(18)F]PI-2620 perfusion imaging in progressive supranuclear palsy and corticobasal syndrome. *Eur J Nucl Med Mol Imaging*. Jan 2023;50(2):423-434. doi:10.1007/s00259-022-05964-w

18. Brendel M, Barthel H, van Eimeren T*, et al*. Assessment of 18F-PI-2620 as a Biomarker in Progressive Supranuclear Palsy. *JAMA Neurol*. Nov 1 2020;77(11):1408-1419. doi:10.1001/jamaneurol.2020.2526

19. Palleis C, Brendel M, Finze A*, et al*. Cortical [(18) F]PI-2620 Binding Differentiates Corticobasal Syndrome Subtypes. *Mov Disord*. Sep 2021;36(9):2104-2115. doi:10.1002/mds.28624

20. Meyer PT, Frings L, Rucker G, Hellwig S. (18)F-FDG PET in Parkinsonism: Differential Diagnosis and Evaluation of Cognitive Impairment. *J Nucl Med*. Dec 2017;58(12):1888-1898. doi:10.2967/jnumed.116.186403

21. Beyer L, Meyer-Wilmes J, Schonecker S*, et al*. Clinical Routine FDG-PET Imaging of Suspected Progressive Supranuclear Palsy and Corticobasal Degeneration: A Gatekeeper for Subsequent Tau-PET Imaging? *Front Neurol*. 2018;9:483. doi:10.3389/fneur.2018.00483

22. Pardini M, Huey ED, Spina S*, et al*. FDG-PET patterns associated with underlying pathology in corticobasal syndrome. *Neurology*. Mar 5 2019;92(10):e1121-e1135. doi:10.1212/WNL.0000000000007038

23. Eckert T, Barnes A, Dhawan V*, et al*. FDG PET in the differential diagnosis of parkinsonian disorders. *Neuroimage*. Jul 1 2005;26(3):912-21. doi:10.1016/j.neuroimage.2005.03.012

24. Tang CC, Poston KL, Eckert T*, et al*. Differential diagnosis of parkinsonism: a metabolic imaging study using pattern analysis. *Lancet Neurol*. Feb 2010;9(2):149-58. doi:10.1016/S1474-4422(10)70002-8

25. Carrera E, Tononi G. Diaschisis: past, present, future. *Brain*. Sep 2014;137(Pt 9):2408-22. doi:10.1093/brain/awu101

26. Feeney DM, Baron JC. Diaschisis. *Stroke*. Sep-Oct 1986;17(5):817-30. doi:10.1161/01.str.17.5.817

27. Kempinsky WH. Vascular and neuronal factors in diaschisis with focal cerebral ischemia. *Res Publ Assoc Res Nerv Ment Dis*. 1966;41:92-115.

28. Provost K, La Joie R, Strom A*, et al*. Crossed cerebellar diaschisis on (18)F-FDG PET: Frequency across neurodegenerative syndromes and association with (11)C-PIB and (18)F-Flortaucipir. *J Cereb Blood Flow Metab*. Sep 2021;41(9):2329-2343. doi:10.1177/0271678X211001216

29. Beyer L, Nitschmann A, Barthel H*, et al*. Early-phase [(18)F]PI-2620 tau-PET imaging as a surrogate marker of neuronal injury. *Eur J Nucl Med Mol Imaging*. Nov 2020;47(12):2911-2922. doi:10.1007/s00259-020-04788-w

30. Volter F, Beyer L, Eckenweber F*, et al*. Assessment of perfusion deficit with early phases of [(18)F]PI-2620 tau-PET versus [(18)F]flutemetamol-amyloid-PET recordings. *Eur J Nucl Med Mol Imaging*. Apr 2023;50(5):1384-1394. doi:10.1007/s00259-022-06087-y

31. Pichet Binette A, Franzmeier N, Spotorno N*, et al*. Amyloid-associated increases in soluble tau relate to tau aggregation rates and cognitive decline in early Alzheimer's disease. *Nat Commun*. Nov 4 2022;13(1):6635. doi:10.1038/s41467-022-34129-4

32. Frontzkowski L, Ewers M, Brendel M*, et al*. Earlier Alzheimer's disease onset is associated with tau pathology in brain hub regions and facilitated tau spreading. *Nat Commun*. Aug 20 2022;13(1):4899. doi:10.1038/s41467-022-32592-7

33. Armstrong MJ, Litvan I, Lang AE*, et al*. Criteria for the diagnosis of corticobasal degeneration. *Neurology*. Jan 29 2013;80(5):496-503. doi:10.1212/WNL.0b013e31827f0fd1

34. Avants BB, Tustison NJ, Song G, Cook PA, Klein A, Gee JC. A reproducible evaluation of ANTs similarity metric performance in brain image registration. *Neuroimage*. Feb 1 2011;54(3):2033-44. doi:10.1016/j.neuroimage.2010.09.025

35. Tian Y, Margulies DS, Breakspear M, Zalesky A. Topographic organization of the human subcortex unveiled with functional connectivity gradients. *Nat Neurosci*. Nov 2020;23(11):1421-1432. doi:10.1038/s41593-020-00711-6

36. Schaefer A, Kong R, Gordon EM*, et al*. Local-Global Parcellation of the Human Cerebral Cortex from Intrinsic Functional Connectivity MRI. *Cereb Cortex*. Sep 1 2018;28(9):3095-3114. doi:10.1093/cercor/bhx179

37. Franzmeier N, Dehsarvi A, Steward A*, et al*. Elevated CSF GAP-43 is associated with accelerated tau accumulation and spread in Alzheimer's disease. *Nat Commun*. Jan 3 2024;15(1):202. doi:10.1038/s41467-023-44374-w

38. Franzmeier N, Dewenter A, Frontzkowski L*, et al*. Patient-centered connectivity-based prediction of tau pathology spread in Alzheimer's disease. *Sci Adv*. Nov 2020;6(48)doi:10.1126/sciadv.abd1327

39. Franzmeier N, Neitzel J, Rubinski A*, et al*. Functional brain architecture is associated with the rate of tau accumulation in Alzheimer's disease. *Nat Commun*. Jan 17 2020;11(1):347. doi:10.1038/s41467-019-14159-1

40. Franzmeier N, Rubinski A, Neitzel J*, et al*. Functional connectivity associated with tau levels in ageing, Alzheimer's, and small vessel disease. *Brain*. Apr 1 2019;142(4):1093-1107. doi:10.1093/brain/awz026

41. Steward A, Biel D, Brendel M*, et al*. Functional network segregation is associated with attenuated tau spreading in Alzheimer's disease. *Alzheimers Dement*. May 2023;19(5):2034-2046. doi:10.1002/alz.12867

42. Steward A, Biel D, Dewenter A*, et al*. ApoE4 and Connectivity-Mediated Spreading of Tau Pathology at Lower Amyloid Levels. *JAMA Neurol*. Nov 6 2023;doi:10.1001/jamaneurol.2023.4038

43. Vogel JW, Corriveau-Lecavalier N, Franzmeier N*, et al*. Connectome-based modelling of neurodegenerative diseases: towards precision medicine and mechanistic insight. *Nat Rev Neurosci*. Oct 2023;24(10):620-639. doi:10.1038/s41583-023-00731-8

44. Lopez-Gonzalez FJ, Paredes-Pacheco J, Thurnhofer-Hemsi K*, et al*. QModeling: a Multiplatform, Easy-to-Use and Open-Source Toolbox for PET Kinetic Analysis. *Neuroinformatics*. Jan 2019;17(1):103-114. doi:10.1007/s12021-018-9384-y

45. Landau SM, Mintun MA, Joshi AD*, et al*. Amyloid deposition, hypometabolism, and longitudinal cognitive decline. *Ann Neurol*. Oct 2012;72(4):578-86. doi:10.1002/ana.23650

46. Maass A, Landau S, Baker SL*, et al*. Comparison of multiple tau-PET measures as biomarkers in aging and Alzheimer's disease. *Neuroimage*. Aug 15 2017;157:448-463. doi:10.1016/j.neuroimage.2017.05.058

47. Franzmeier N, Dewenter A, Frontzkowski L*, et al*. Patient-centered connectivity-based prediction of tau patholog spread in Alzheimer’s disease. *Sci Adv*. 2020;

48. Steward A, Biel D, Brendel M*, et al*. Functional network segregation is associated with attenuated tau spreading in Alzheimer's disease. *Alzheimers Dement*. Nov 25 2022;doi:10.1002/alz.12867

49. *R: A language and environment for statistical computing*. R Foundation for Statistical Computing; 2021. https://www.R-project.org/

50. Messerschmidt K, Barthel H, Brendel M*, et al*. (18)F-PI-2620 Tau PET Improves the Imaging Diagnosis of Progressive Supranuclear Palsy. *J Nucl Med*. Nov 2022;63(11):1754-1760. doi:10.2967/jnumed.121.262854

51. Zhao P, Zhang B, Gao S, Li X. Clinical, MRI and 18F-FDG-PET/CT analysis of progressive supranuclear palsy. *J Clin Neurosci*. Oct 2020;80:318-323. doi:10.1016/j.jocn.2020.06.008

52. Smith R, Scholl M, Honer M, Nilsson CF, Englund E, Hansson O. Tau neuropathology correlates with FDG-PET, but not AV-1451-PET, in progressive supranuclear palsy. *Acta Neuropathol*. Jan 2017;133(1):149-151. doi:10.1007/s00401-016-1650-1

53. Lanciego JL, Luquin N, Obeso JA. Functional neuroanatomy of the basal ganglia. *Cold Spring Harb Perspect Med*. Dec 1 2012;2(12):a009621. doi:10.1101/cshperspect.a009621

54. Behrens TE, Johansen-Berg H, Woolrich MW*, et al*. Non-invasive mapping of connections between human thalamus and cortex using diffusion imaging. *Nat Neurosci*. Jul 2003;6(7):750-7. doi:10.1038/nn1075

55. Gendron TF, Petrucelli L. The role of tau in neurodegeneration. *Mol Neurodegener*. Mar 11 2009;4:13. doi:10.1186/1750-1326-4-13

56. Aghakhanyan G, Rullmann M, Rumpf J*, et al*. Interplay of tau and functional network connectivity in progressive supranuclear palsy: a [(18)F]PI-2620 PET/MRI study. *European journal of nuclear medicine and molecular imaging*. Dec 2022;50(1):103-114. doi:10.1007/s00259-022-05952-0

57. Kwan LT, Reed BR, Eberling JL*, et al*. Effects of subcortical cerebral infarction on cortical glucose metabolism and cognitive function. *Arch Neurol*. Jul 1999;56(7):809-14. doi:10.1001/archneur.56.7.809

58. Perani D, Vallar G, Cappa S, Messa C, Fazio F. Aphasia and neglect after subcortical stroke. A clinical/cerebral perfusion correlation study. *Brain*. Oct 1987;110 (Pt 5):1211-29. doi:10.1093/brain/110.5.1211

59. Hillis AE, Wityk RJ, Barker PB*, et al*. Subcortical aphasia and neglect in acute stroke: the role of cortical hypoperfusion. *Brain*. May 2002;125(Pt 5):1094-104. doi:10.1093/brain/awf113

60. Volter F, Beyer L, Eckenweber F*, et al*. Assessment of perfusion deficit with early phases of [(18)F]PI-2620 tau-PET versus [(18)F]flutemetamol-amyloid-PET recordings. *Eur J Nucl Med Mol Imaging*. Dec 27 2022;doi:10.1007/s00259-022-06087-y

61. Leuzy A, Binette AP, Vogel JW*, et al*. Comparison of Group-Level and Individualized Brain Regions for Measuring Change in Longitudinal Tau Positron Emission Tomography in Alzheimer Disease. *JAMA Neurol*. Jun 1 2023;80(6):614-623. doi:10.1001/jamaneurol.2023.1067

62. Kouri N, Whitwell JL, Josephs KA, Rademakers R, Dickson DW. Corticobasal degeneration: a pathologically distinct 4R tauopathy. *Nat Rev Neurol*. May 2011;7(5):263-72. doi:10.1038/nrneurol.2011.43

63. Wu JW, Hussaini SA, Bastille IM, *et al*. Neuronal activity enhances tau propagation and tau pathology in vivo. *Nat Neurosci*. Aug 2016;19(8):1085-92. doi:10.1038/nn.4328

64. Wang Y, Balaji V, Kaniyappan S*, et al*. The release and trans-synaptic transmission of Tau via exosomes. *Mol Neurodegener*. Jan 13 2017;12(1):5. doi:10.1186/s13024-016-0143-y

65. Franzmeier N, Neitzel J, Rubinski A*, et al*. Functional brain architecture is associated with the rate of tau accumulation in Alzheimer's disease. *Nat Commun*. Jan 17 2020;11(1):347. doi:10.1038/s41467-019-14159-1

66. Song M, Beyer L, Kaiser L*, et al*. Binding characteristics of [(18)F]PI-2620 distinguish the clinically predicted tau isoform in different tauopathies by PET. *J Cereb Blood Flow Metab*. Nov 2021;41(11):2957-2972. doi:10.1177/0271678X211018904

67. Honey CJ, Sporns O, Cammoun L*, et al*. Predicting human resting-state functional connectivity from structural connectivity. *Proc Natl Acad Sci U S A*. Feb 10 2009;106(6):2035-40. doi:10.1073/pnas.0811168106

68. Abhinav K, Yeh FC, Pathak S, *et al*. Advanced diffusion MRI fiber tracking in neurosurgical and neurodegenerative disorders and neuroanatomical studies: A review. *Biochim Biophys Acta*. Nov 2014;1842(11):2286-2297. doi:10.1016/j.bbadis.2014.08.002

69. Ji JL, Spronk M, Kulkarni K, Repovs G, Anticevic A, Cole MW. Mapping the human brain's cortical-subcortical functional network organization. *Neuroimage*. Jan 15 2019;185:35-57. doi:10.1016/j.neuroimage.2018.10.006

70. Finn ES, Shen X, Scheinost D, *et al*. Functional connectome fingerprinting: identifying individuals using patterns of brain connectivity. *Nat Neurosci*. Nov 2015;18(11):1664-71. doi:10.1038/nn.4135

Figure legends

Figure 1 Spatial mapping of abnormal tau-PET (A) and abnormal perfusion-PET (B) across the 51 PSP/CBS patients. Abnormality was defined as the probability of z-scores crossing pre-established z-score threshold of 1.5 for tau-PET and -1.5 for perfusion-PET. Tau-PET images were intensity normalized to an inferior cerebellar reference, perfusion-PET images were normalized to a Pons reference.

Figure 2 Scatterplot illustrating the association between tau-PET z-scores in the tau epicenter and cortical perfusion-PET z-scores for global (A) and regional perfusion-PET data (B; regions of non-significant association are depicted in grey)

Figure 3 Illustration of the workflow to determine whether the connectivity of subcortical tau epicenters predicts cortical hypoperfusion patterns. For group-level data, subcortical tau epicenters were determined as 10% of ROIs with highest tau-PET z-scores (A). Using the resting-state fMRI connectivity template determined in the 69 healthy control subjects, we assessed seed-based connectivity of the subcortical tau epicenters to the cortex (B) and assessed mean perfusion-

PET z-scores across the sample of 51 4R tauopathy patients (C). The association between tau epicenter connectivity and cortical perfusion-PET z-scores is illustrated in the scatter-plot (D). Note that connectivity is displayed as connectivity distance, where shorter distance indicates stronger connectivity. The same analyses were performed on subject-level data, yielding a regression-derived beta-value for the association between tau epicenter connectivity and cortical perfusion controlling for cortical tau-PET levels. The distribution of beta-values is shown in the boxplot (E), illustrating that regions more strongly connected to the epicenter show stronger perfusion reductions (i.e. positive beta-values as in panel D).

Figure 4 Subcortical tau epicenters were defined for each subject, and cortical ROIs were grouped into 4 quartiles (i.e. Q1-Q4) depending on the connectivity strength to the subject-specific tau epicenter, with Q1 showing the strongest connectivity to the epicenter. The boxplot illustrates that regions more closely connected to the tau epicenter showed stronger hypoperfusion than regions that were less strongly connected to the tau epicenters. P-values were determined based on paired t-tests.

Table 1 Study cohort and demographics

	CBS (n=25)	PSP[a] (n=26)	p-value
Age	70.7 ± 5.70	70.5 ± 7.14	0.938
Sex (f/m)	15/10	10/16	0.208
PSPRS[b]	27.2 ± 11.0	27.6 ± 14.9	0.944
MoCA[c]	20.8 ± 5.22	23.8 ± 3.58	0.174
SEADL[d]	60.0 ± 18.9	65.8 ± 20.2	0.493

Mean distribution and standard deviation of age, sex, PSPRS, MoCA and SEADL across the CBS and PSP study cohort. T-tests did not yield any significant differences between PSP and CBS patients.
[a]Diagnoses: PSP-Richardson Syndrome, n=19; PSP Progressive Gait Freezing, n=1, PSP Parkinsonism, n=2, PSP Speech/Language Variant, n=4.
[b]PSPRS available for 20/51 subjects.
[c]MoCA available for 27/51 subjects.
[d]SEADL available for 22/51 subjects.

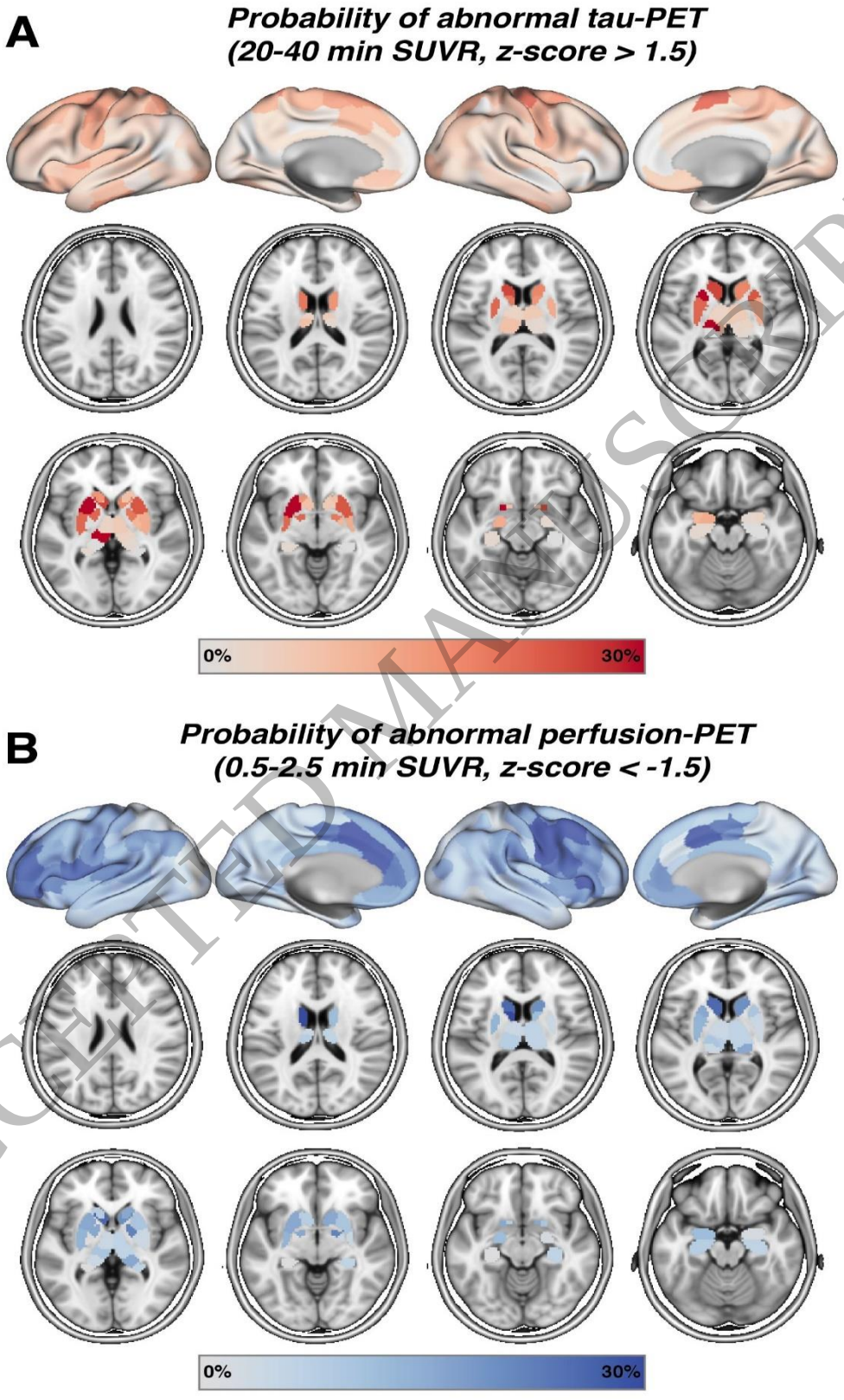

Figure 1
139x246 mm (DPI)

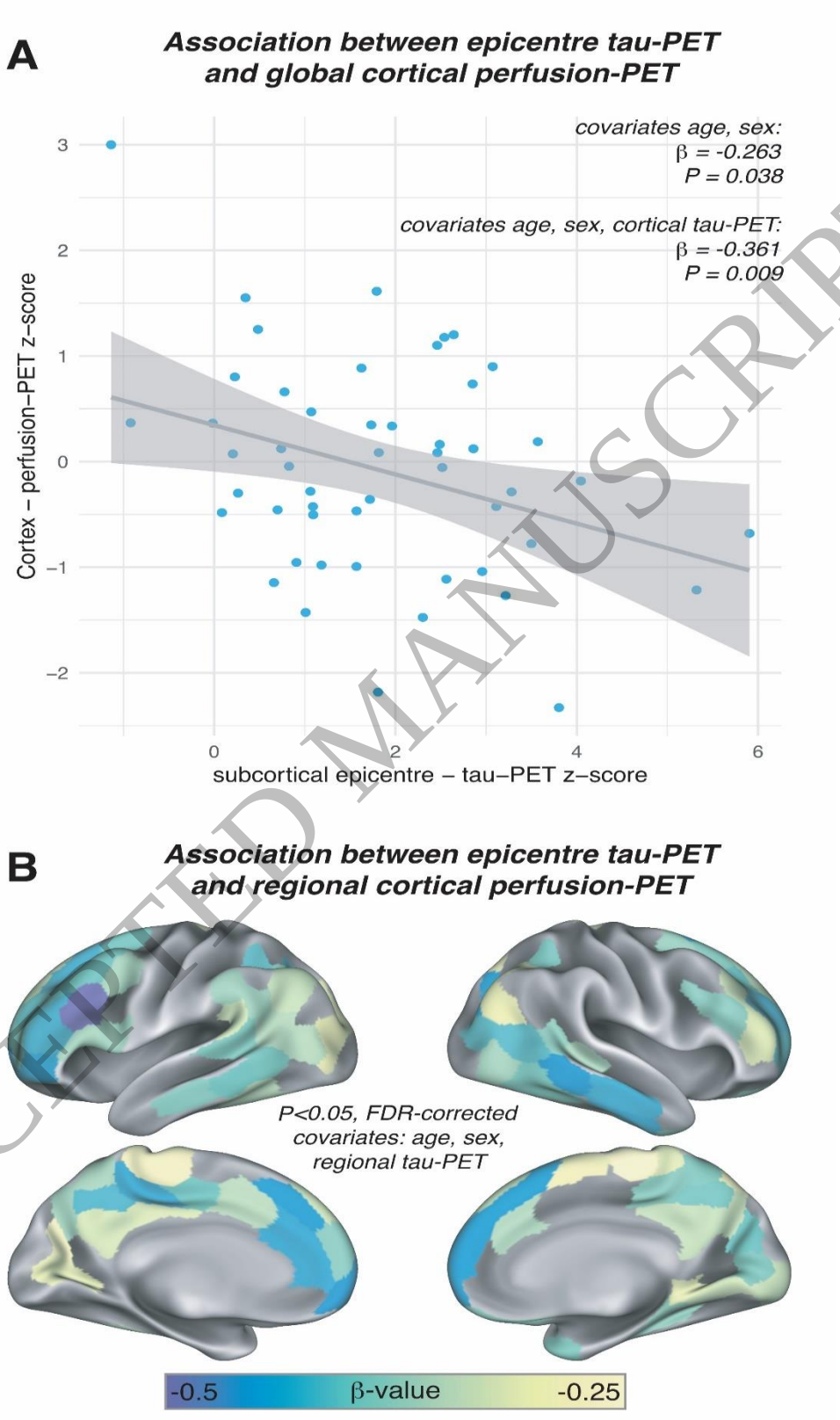

Figure 2
130x246 mm (DPI)

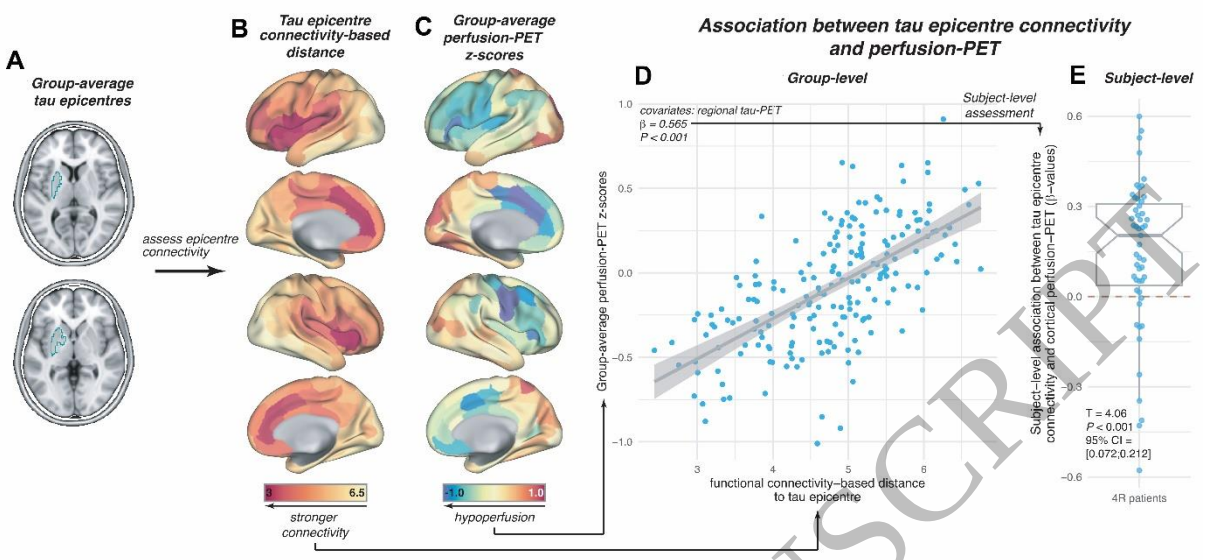

Figure 3
159x75 mm (DPI)

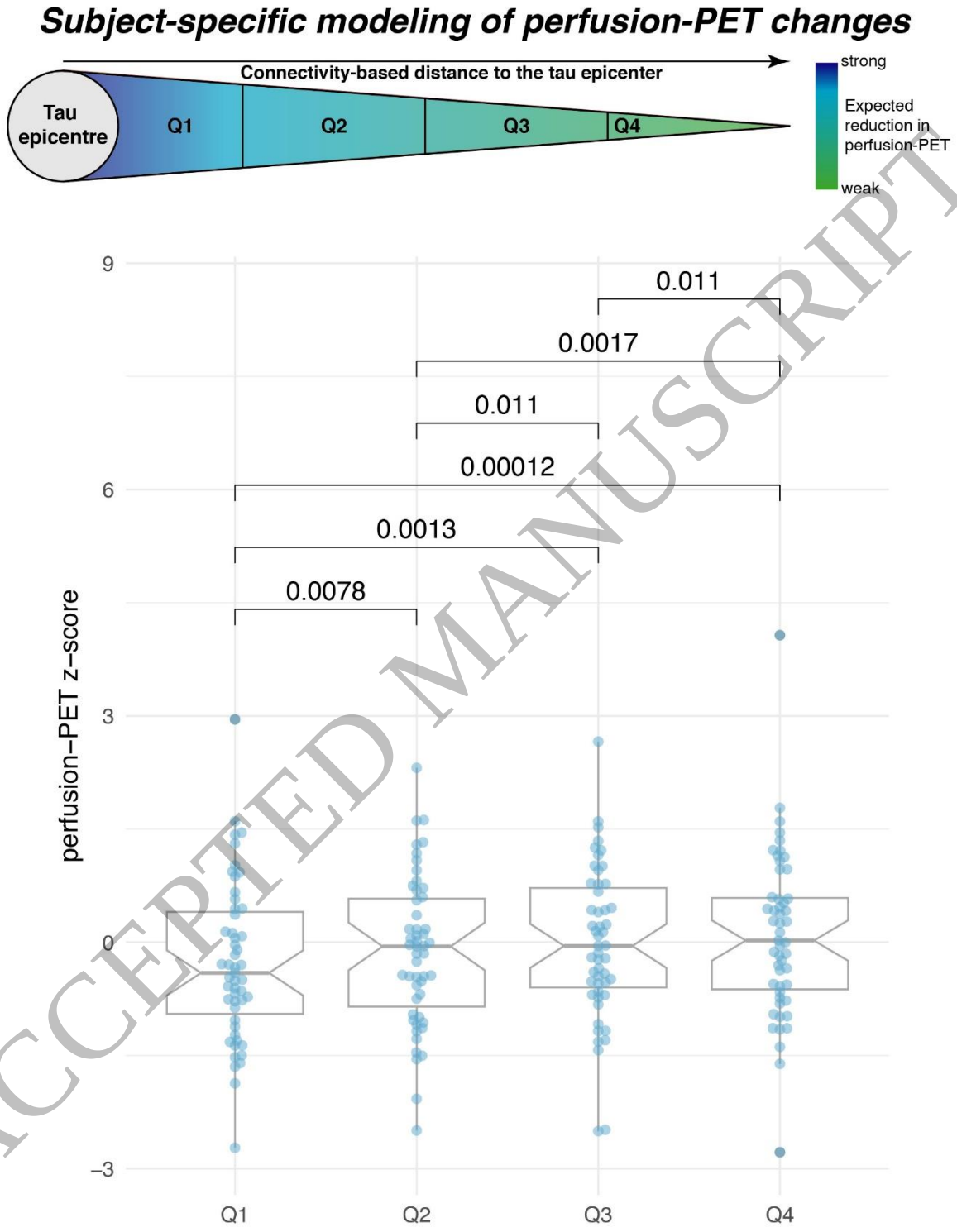

Figure 4
159x208 mm (DPI)